Measurement and Numerical Simulation of Three-Dimensional Fiber Orientation States in Injection-Molded Short-Fiber-Reinforced Plastics

Kwang Seok Lee, Seok Won Lee, Kwansoo Chung, Tae Jin Kang, Jae Ryoun Youn

School of Materials Science and Engineering, Seoul National University, Seoul, 151-742, South Korea

Received 7 January 2002; accepted 6 June 2002

ABSTRACT: To determine three-dimensional fiber orientation states in injection-molded short-fiber composites, a confocal laser scanning microscope (CLSM) is used. Since the CLSM optically sections the specimen, more than two images of the cross sections on and below the surface of the composite can be obtained. Three-dimensional fiber orientation states can be determined by using geometric parameters of fiber images obtained from two parallel cross sections. For experiments, carbon-fiber-reinforced polystyrene is examined by the CLSM and geometric parameters of fibers on each cross-sectional plane are measured by an image analysis. In order to describe fiber orientation states compactly, orientation tensors are determined at different positions of the prepared specimen. Three-dimensional orientation states are obtained without any difficulty by determining the out-of-plane angles utilizing fiber images on two parallel planes acquired by the CLSM. Orientation states are different at different positions and show the shell–core structure along the thickness of the specimen. Fiber orientation tensors are predicted by a numerical analysis and the numerically predicted orientation states show good agreement with measured ones. However, some differences are found at the end of cavity. They may result from the fountain flow effects, which are not considered in the numerical analysis.
 J Appl Polym Sci 88: 500–509, 2003

Key words: composites; fibers; imaging; injection molding; orientation

INTRODUCTION

Short-fiber-reinforced plastics (SFRP) are being widely used for technical and industrial applications due to good mechanical properties, easiness of manufacturing, and economical advantages. SFRP are usually processed by injection molding or compression molding. During molding, a complex flow field is generated in the cavity and the fiber orientation depends highly on the process conditions.[1–3] Fiber orientation in SFRP controls mechanical and thermal properties[4] of the final product, such as stiffness, tribology,[5–7] thermal expansion, and strength. Therefore, it is important to measure the fiber orientation in real composite parts and to apply the measured fiber orientation states to characterization of local properties. Fiber orientation states can be predicted by numerical simulations and orientation tensors are frequently used to express the fiber orientation states.

Many different methods have been developed to determine the fiber orientation in SFRP experimentally. Among them, reflective microscopy is the most popular method for measurement of fiber orientation. It can produce fiber images from surfaces prepared by metallographic polishing. If the cross section of the fiber is circular, an elliptical image of fiber cross section will appear on the intercepting plane. Directional angles (θ, ϕ) of fibers can be calculated by measuring the principal axes of the ellipse as shown in Figure 1. However, this method has some weak points. First, there always exists the ambiguity of out-of-plane angle (θ) because both elliptical images of fibers oriented at angle θ and of fibers oriented at angle $180° - \theta$ are identical. Second, as the cross section of fiber is getting closer to a perfect circle, the sensitivity in the measurement of out-of-plane angle (θ) is increasing, which could lead to serious errors. In order to minimize the error, resolution of the measuring instrument should be high enough. Yurgartis[8] and other researchers[9,10] sectioned specimens at an angle with respect to the melt flow direction. Although this way of sectioning can dramatically reduce the second error, the first problem still remains unsolved. Fortunately, the ambiguity can be removed by an optical sectioning technique, where parallel planes below the surface are captured by focusing the laser beam at different depth.[11] Thomason and Knoester[12] proposed that a confocal laser scanning microscope be used for the

Correspondence to: Jae Ryoun Youn (jaeryoun@gong.snu.ac.kr).

Contract grant sponsor: the Korea Science and Engineering Foundation through the Applied Rheology Center.

Contract grant sponsor: the Ministry of Science and Technology through the National Research Laboratory.

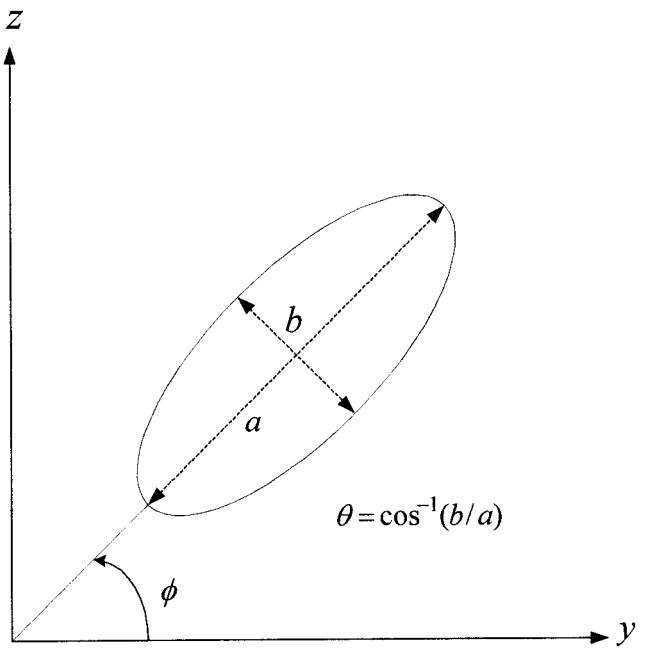

Figure 1 Elliptical image of a fiber on the sectioning plane.

study of fiber-reinforced polymer composites. By using the confocal laser scanning microscope (CLSM),[13] more than two parallel planes below the surface can be focused so that the ambiguity can be eliminated in determining the out-of-plane angles.

In this study, three-dimensional fiber orientation tensors are determined by determining the angles without any difficulty. For experiments, tensile specimens are injection-molded with polystyrene reinforced by 3 vol % (4.5 wt %) short carbon fibers. The specimen is examined by the CLSM at different positions and across the thickness of the specimen. By measuring the center coordinates of the elliptical fiber images appearing on the micrographs, the directional angles of fibers are determined. Finally, orientation tensors are calculated with the directional angles. Measured tensors are also compared with numerically predicted tensors so as to verify numerical results.

THEORETICAL

Description of fiber orientation

Assuming that the fiber is rigid and uniform in length, the orientation of fibers can be represented by using unit vectors **p** directed toward the end of fibers, as shown in Figure 2. The components of **p** are related to θ and ϕ:

$$\begin{aligned} \mathbf{p}_1 &= \cos\theta \\ \mathbf{p}_2 &= \sin\theta\cos\phi \\ \mathbf{p}_3 &= \sin\theta\sin\phi \end{aligned} \tag{1}$$

Since two ends of the fiber are not distinguishable, the following relation holds:

$$\mathbf{p} = -\mathbf{p} \tag{2}$$

Since the fibers in SFRP are lying toward more than one direction and do not have uniform length, a description that reflects the orientation of many single fibers and variation of the length is required. One approach is to use the probability density function ψ, which gives the probability of a fiber being oriented at angles between θ_0 and $\theta_0 + d\theta$, ϕ_0 and $\phi_0 + d\phi_0$ having a length between L_0 and $L_0 + dL$, as follows:

$$\begin{aligned} P(\theta_0 \le \theta \le \theta_0 + d\theta,\ \phi_0 \le \phi_0 + d\phi,\ L_0 \le L \le L_0 + dL) \\ = \psi(\theta_0, \phi_0, L_0)\sin\theta_0 d\theta d\phi dL \end{aligned} \tag{3}$$

Since every fiber is oriented at some angle and has some length, the integration of the probability density function over all angles and every possible length must be equal to unity:

$$\int_{\mathbf{p}}\int_{L} \psi(\mathbf{p}, L)dLd\mathbf{p} = 1 \tag{4}$$

According to eq. (2), the distribution function must e an even function:

$$\psi(\mathbf{p}, L) = \psi(-\mathbf{p}, L) \tag{5}$$

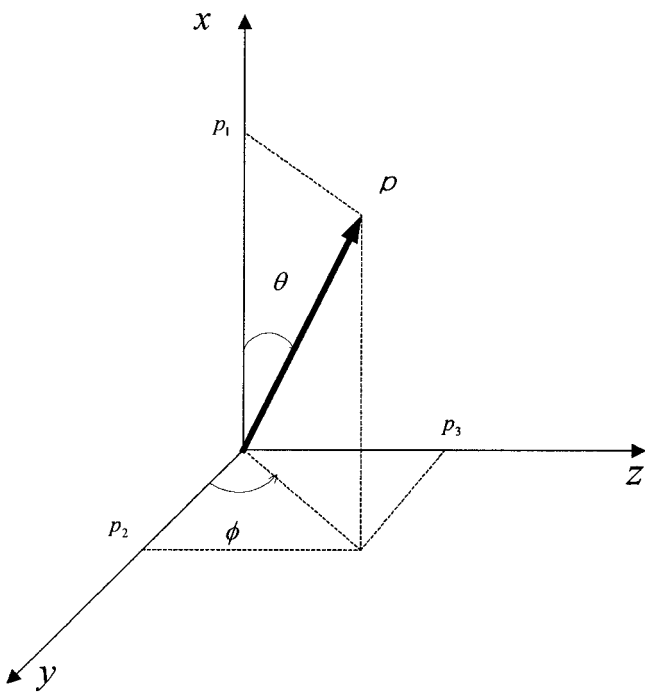

Figure 2 Coordinate system employed for expression of the fiber orientation.

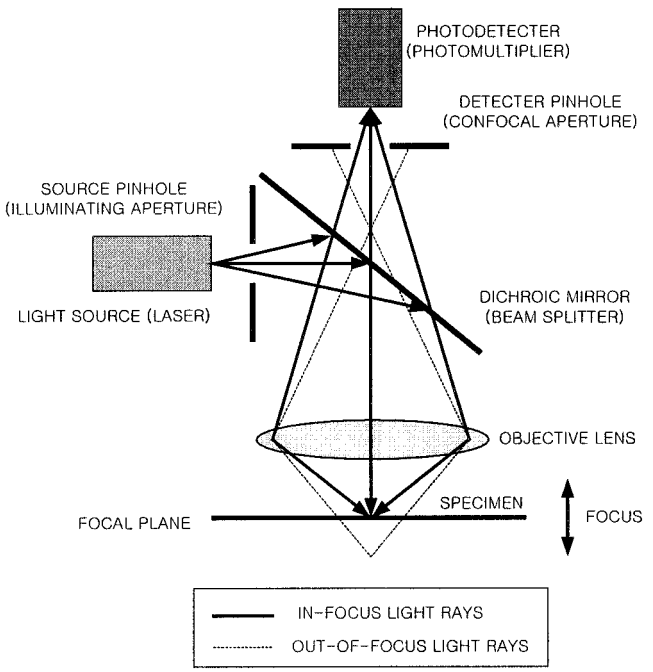

Figure 3 Simplified optics of a confocal laser scanning microscope.

Equation (5) is called the periodic condition. The distribution function ψ (**p**,L) is a general description of the orientation state. Because it is not practical to calculate ψ (**p**,L) in such an application as numerical analysis, a more compact and efficient description is needed.

Another approach is to use the orientation tensors that are created by forming dyadic products of the vector **p** and integrating over all directions and every possible length by weighting the dyadic product with the distribution function ψ and the length L. The second orientation tensor is defined as follows:

$$a_{ij} = \frac{\int_L \int_p p_i p_j L \psi(\mathbf{p}, L) d\mathbf{p} dL}{\int_L \int_p L \psi(\mathbf{p}, L) d\mathbf{p} dL} \tag{6}$$

From the definition, components of orientation tensors follow the transformation rules for tensors. The orientation tensors are symmetric[14]:

$$a_{ij} = a_{ji} \tag{7}$$

From the normalization condition, trace of the second order tensor equals unity:

$$a_{ii} = 1 \tag{8}$$

In actual composites, position vectors and lengths of discrete fiber samples are measured and components of the orientation tensors are calculated by summation as follows:

$$a_{ij} = \frac{\sum (p_i p_j) L_n F'_n}{\sum L_n F'_n} \tag{9}$$

where F'_n represents the weighting function for the nth fiber[15]:

$$F'_n = \frac{1}{L_n \cos \theta_n} \tag{10}$$

$$F'_n = \frac{1}{d_n} \text{ for } \theta_n = 90° \tag{11}$$

where L_n is the length and d_n is the diameter of the n-th fiber.

The weighting function is required because the fiber oriented normal to the sectioning plane is more likely to intercept the plane than the fiber oriented parallel to the plane. F_n also represents the projected height of the fiber onto the axis normal to the sectioning plane. In the case of fibers lying perfectly parallel to the sectioning plane, the fiber diameter

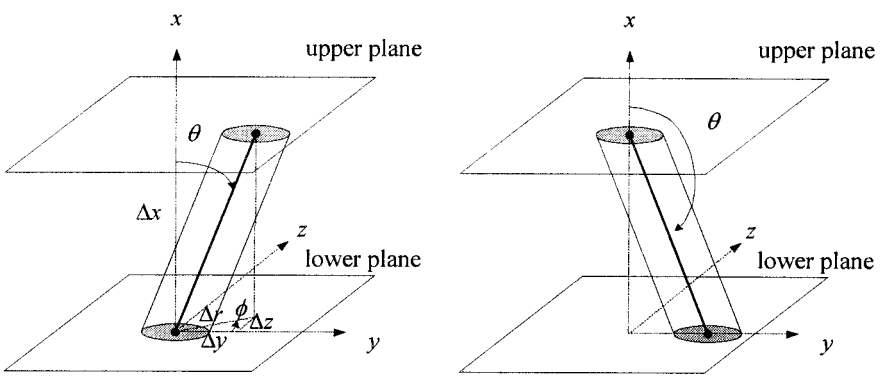

Figure 4 Coordinate system employed to define the directional angles.

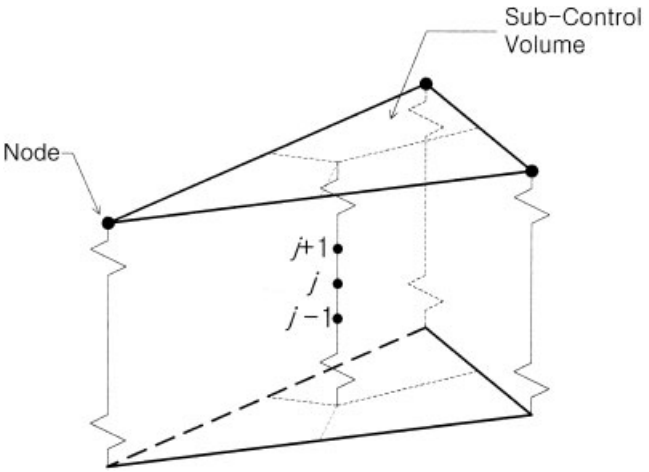

Figure 5 Triangular finite element and finite difference grids in the thickness direction.

can be substituted for the height of fiber. Therefore, eq. (9) becomes

$$a_{ij} = \frac{\sum (p_i p_j) F_n}{\sum F_n} \tag{12}$$

where

$$F_n = \frac{1}{\cos \theta_n} \tag{13}$$

$$F_n = L_n / d_n \text{ for } \theta_n = 90° \tag{14}$$

Principles of confocal laser scanning microscopy

Simplified optics of the CLSM[16,17] is shown schematically in Figure 3. A laser beam from either argon or krypton laser goes through a dichroic mirror (beam splitter) and microscope optics and illuminates a sample. The reflected light and any fluorescence emission from the sample return through the microscope optics, the beam splitter, an emission filter, and a detecter pinhole (confocal aperture) before reaching a photodetector (photomultiplier, PMT). The emission filter selects either the reflected light or the longer wavelength fluorescence light. The former is referred to as the reflection mode and the latter as the fluorescence mode. Mirrors scan the laser beam in both X and Y directions so that an optical XY plane should be defined. The role of the confocal aperture is removing out-of-focus light. As the size of the aperture decreases, the regional image of the focal plane becomes thinner. A focal plane may be placed with an accuracy of 1 μm at the sample surface or below the surface by moving the Z-drive on the microscope. In order to achieve high-quality optical sectioning, a high numerical aperture (NA) lens should be used for the microscope objective and the sample should be sufficiently transparent or at least semitransparent.

Calculation of orientation tensors with CLSM

Since the CLSM is capable of optical sectioning, more than two parallel planes within the sample can be examined. Assuming that each image of a single fiber on two parallel planes is identical, the directional angles (θ, ϕ) can be determined by using center coordinates of the two images as shown in Figure 4:

$$\theta = \tan^{-1}\left(\frac{\Delta r}{\Delta x}\right) \text{ for } \Delta y \geq 0 \tag{15}$$

$$\theta = 180° - \tan^{-1}\left(\frac{\Delta r}{\Delta x}\right) \text{ for } \Delta y < 0 \tag{16}$$

$$\phi = \tan^{-1}\left(\frac{\Delta z}{\Delta y}\right) \tag{17}$$

where

$$\Delta r = \sqrt{\Delta y^2 + \Delta z^2}. \tag{18}$$

Δy and Δz are the differences between the center coordinates of two images:

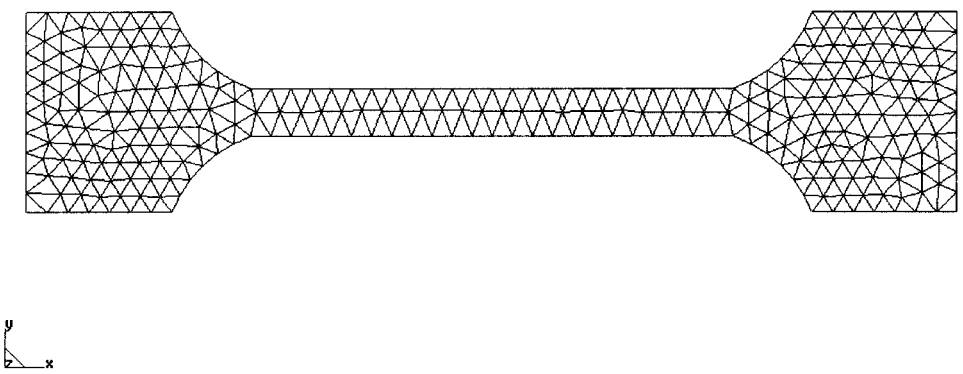

Figure 6 Finite element mesh employed for flow and orientation simulations.

TABLE I
Methods and Conditions Employed for Numerical Analysis

Materials	Polystyrene and carbon fiber
Pressure and temperature	Hybrid FEM/FDM
Melt front advancement	Control volume method
Fiber orientation	Fourth-order Runge–Kutta method
Injection pressure	8 MPa
Holding pressure	7.5 MPa
Filling time	1.6 s
Holding time	5 s
Inlet temperature	200°C
Wall temperature	60°C
C_I (interaction coefficient)	0.01
Inlet fiber orientation	Random state
Total number of elements	488
Total number of nodes	305
Total number of layers	21

$$\Delta y = y_{\text{upper}} - y_{\text{lower}} \tag{19}$$

$$\Delta z = z_{\text{upper}} - z_{\text{lower}} \tag{20}$$

Δr is the distance between two center coordinates and Δx is the difference between upper and lower planes.

After determining directional angles, orientation tensors can be calculated by summing the dyadic products weighted with F_n with eqs. (12)–(14). In the case of fibers lying almost parallel to the sectioning plane, two center coordinates of individual fibers are located far apart. In the case of fibers normal to the sectioning plane, two center coordinates of each image of the fiber are identical. In the experiment, fibers oriented between $\theta = 80°$ and $\theta = 110°$ are sensitive to the error mentioned above. To minimize the error, the major and minor axes of fibers oriented at this range are measured and used for determination of the out-of-plane angle (θ). If the major axis is much greater than the minor axis, the out-of-plane angle (θ) is determined as shown in Figure 1.

Numerical prediction of orientation states

For a numerical analysis,[4,18] flow inside the cavity is assumed to be quasi-steady, creeping, nonisothermal, and inelastic. Pressure and temperature fields were obtained by a control volume-based finite element method (FEM)/finite difference method (FDM) hybrid numerical technique. A generalized Hele–Shaw model is used to deal with compressibility of fluid during the

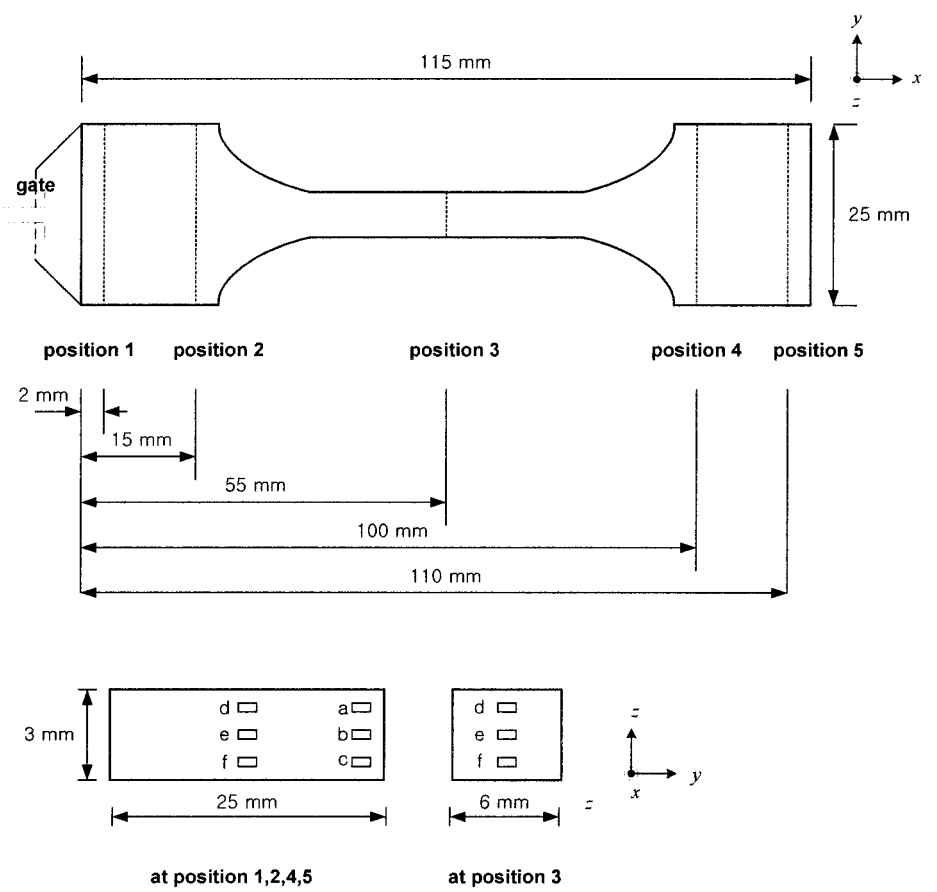

Figure 7 Dimensions of the specimen, sampling positions, and observed locations.

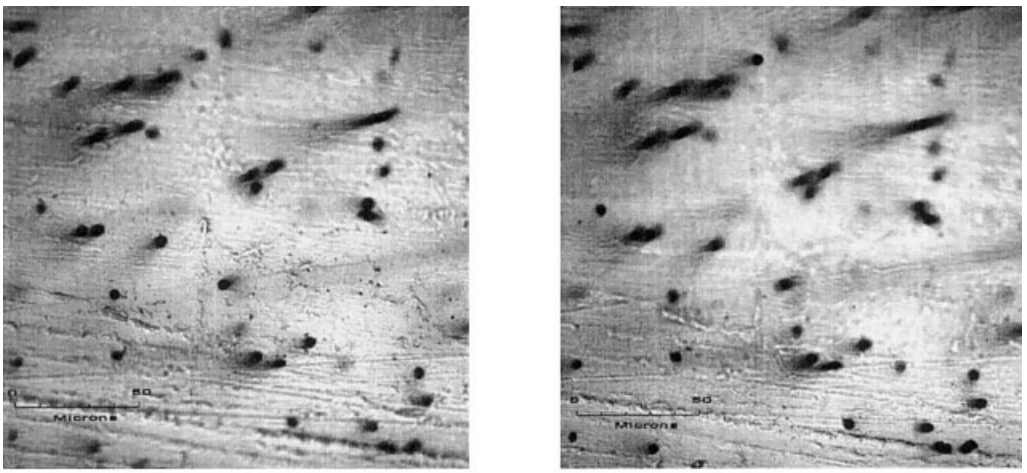

Figure 8 Typical micrographs taken by the CLSM: (a) upper sectioning plane, (b) lower sectioning plane.

injection molding process. Boundary conditions for the nonisothermal flow problem are given as follows: zero pressure at the melt front, impermeable condition at the side wall or insert, and constant volume flow rate at the gate. Non-Newtonian viscosity is described by the modified Cross model. Tait state equation is employed to predict the change of density with respect to pressure and temperature. Fiber orientation is predicted by solving the evolution equation for the second-order orientation tensor. The fourth-order tensor that appears in the evolution equation is approximated by using hybrid closure approximation.[19]

Three-node triangular finite elements as shown in Figure 5 are used. Pressures are calculated at each node and temperature and orientation tensors are calculated at the centroid of each element with respect to the thickness. Figure 6 shows finite element mesh employed for the analysis. Numerical methods, initial conditions, and boundary conditions used for the analysis are summarized in Table I. More specific procedures can be found in the literature.[18]

EXPERIMENTAL

Tensile specimens were injection-molded in order to determine the orientation tenors at different positions. A film-gated cavity is used for molding and geometric dimensions are shown in Figure 7. Samples were prepared from the specimen at different positions. Each sample was optically sectioned by parallel plane with the distance of 1 μm. Geometric parameters of fiber images on two selected parallel planes were measured by using image processing techniques. From measured data the orientation tensors were calculated by using a simple computer code.

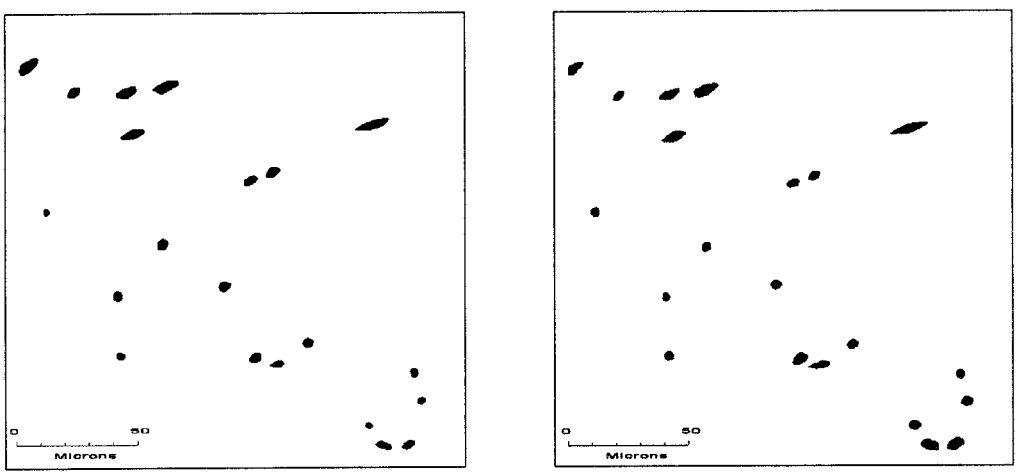

Figure 9 Typical images after thresholding: (a) upper sectioning plane, (b) lower sectioning plane.

Starting materials

For injection molding, 6 mm long chopped carbon fibers (supplied by Taekwang Industrial) and polystyrene (GPPS HF-2680, supplied by Cheil Industries) were used. The average fiber diameter was 6.8 μm according to the supplier's information. Polystyrene reinforced with 3 vol % (4.5 wt %) carbon fiber was compounded by mixing them at 200°C in a twin-screw extruder (PRISM, U.K.) and the extrudates were cut into pellets.

Process conditions for injection molding

The specimens were molded by using an injection molding machine (Battenfeld). The injection pressure was 8 MPa, holding pressure was 7.5 MPa, barrel temperature was 200°C, mold temperature was 60°C, filling time was 1.6 s, holding time was 5 s, and cooling time was 25 s.

Sample preparation and optical sectioning with CLSM

Samples were prepared by cutting the mold specimen normal to the flow direction at five different positions (position 1–5) as shown in Figure 7 and each sample was polished by using the metallographic method.[19] Finer grades of silicon carbide papers were used successively with water to obtain good quality of polishing (320, 800, 1,200, 2,000, 4,000 SiC papers). Final thickness of the sample was about 1 mm. Each sample was placed on the slide glass and squared paper was used to align the samples.

Six locations (*a–f*) on each sample were observed by the CLSM. Three locations (*d–f*) were observed for the sample acquired from position 3. Specific locations of the points are described in Figure 7. Images of 20 to 30 cross sections at each point were obtained by using the optical sectioning technique and the separation between adjacent sectioning planes was 1 μm. For the optical sectioning, Bio-Rad Radian 2000MP was employed with the objective of NA 0.75 ($\times$40 magnification) and the eyepiece of $\times$10 magnification and operated on the transmission mode. Actual size of the observed domain was 187 μm $\times$ 187 μm. The original micrographs obtained by CLSM are shown in Figure 8.

Image processing and calculation of orientation tensor

Two cross sections separated by 10 μm were selected for the image processing.[20–22] The image processing was conducted by using a commercial image analysis tool (Image-Pro Plus 4.1, Media Cybernetics). The sections were first enhanced by controlling the contrast and brightness of images and then transformed into binary images by the thresholding method in order to discard other unnecessary images such as dusts and cracks. The fiber images that overlapped each other due to insufficient axial resolution or the fiber images intercepting the boundary of the domain were removed by manual operation. Figure 9 shows the examples of images after thresholding process.

From fiber images of the two sections, geometric parameters, center coordinates, major axes, minor axes, and in-plane directional angles (ϕ) were measured. The two directional angles (θ, ϕ) of fibers were calculated from the difference between the center coordinates of the upper and lower planes by using eqs. (15)–(20). The orientation tensors are calculated by applying eqs. (12)–(14). In the experiment, cross sections of 10–30 fibers were measured in each section.

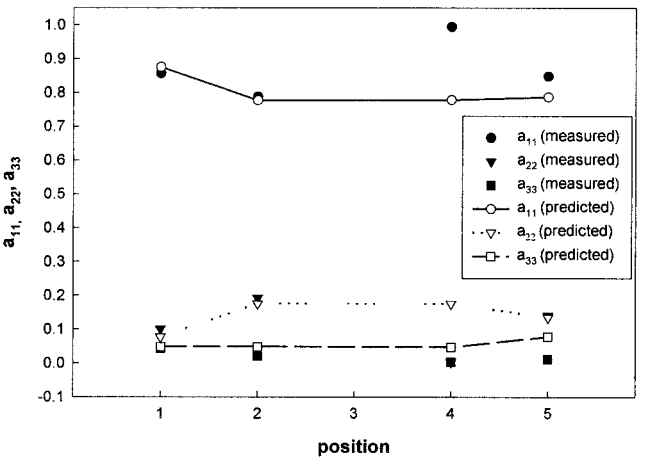

(a)

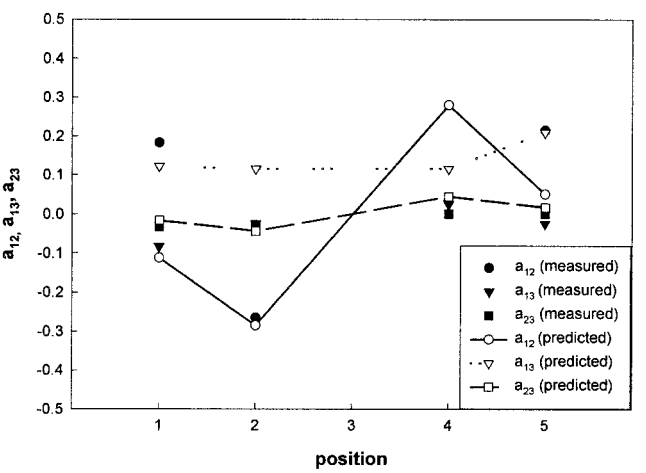

(b)

Figure 10 Measured and predicted orientation tensors along location **a:** (a) diagonal components, (b) off-diagonal components.

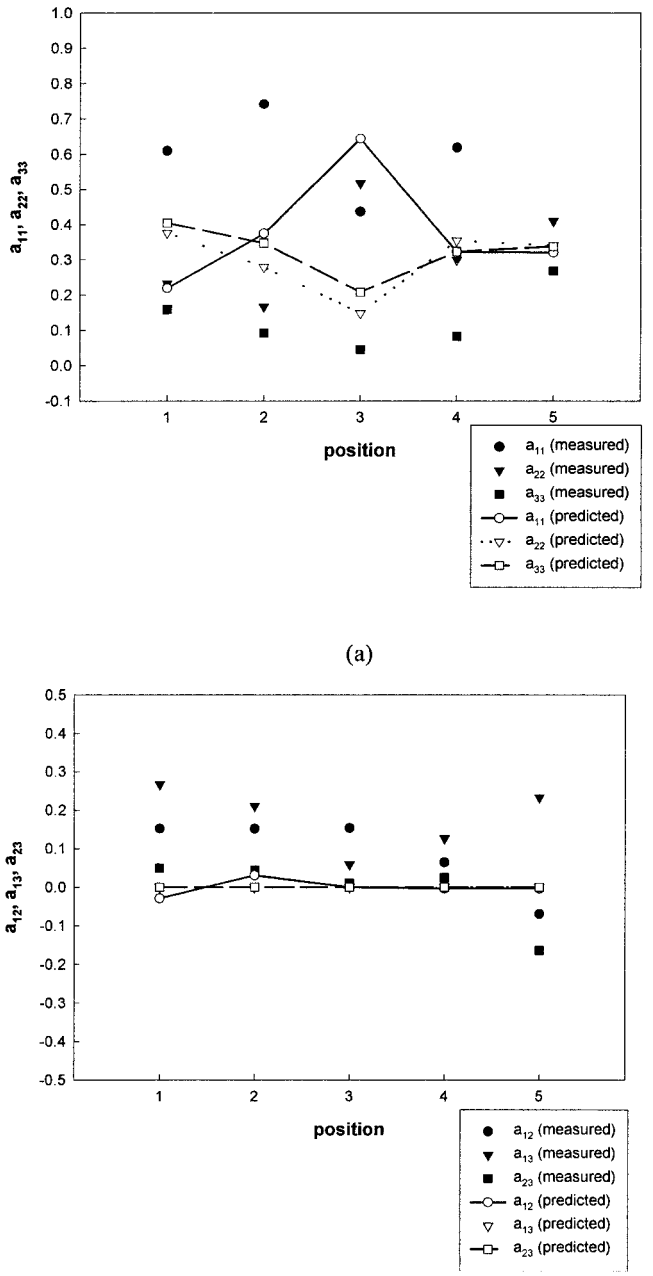

Figure 11 Measured and predicted orientation tensors along location **e:** (a) diagonal terms, (b) off-diagonal terms.

RESULTS AND DISCUSSION

Orientation states along flow direction

Components of measured and predicted orientation tensors along at the edge (location *a*) of the specimen are shown in Figure 10. The measured values of a_{11} components, close to unity along the location *a*, indicate that most of fibers are aligned to the x-direction (flow direction). However, the value of a_{12}, changing from positive at position 1 to negative at position 2, indicates that fibers are rotated toward the converging region of specimen. Figure 11 shows the measured orientation states along the location *e* and indicates that the fibers are more aligned in the flow direction than the predicted states. There is a possibility that the fibers are initially aligned when the polymer melt is transported through the fan-shaped gate. The gate was not considered in the simulation and random orientation state was used as the initial value. In Figure 12, orientation states along the center of the tensile specimen is shown and a_{33}, a_{13}, and a_{23} have small values along location *f* so that the orientation states are almost planar. At the converging region (position 2), fibers are slightly rotated from the x-direction to the

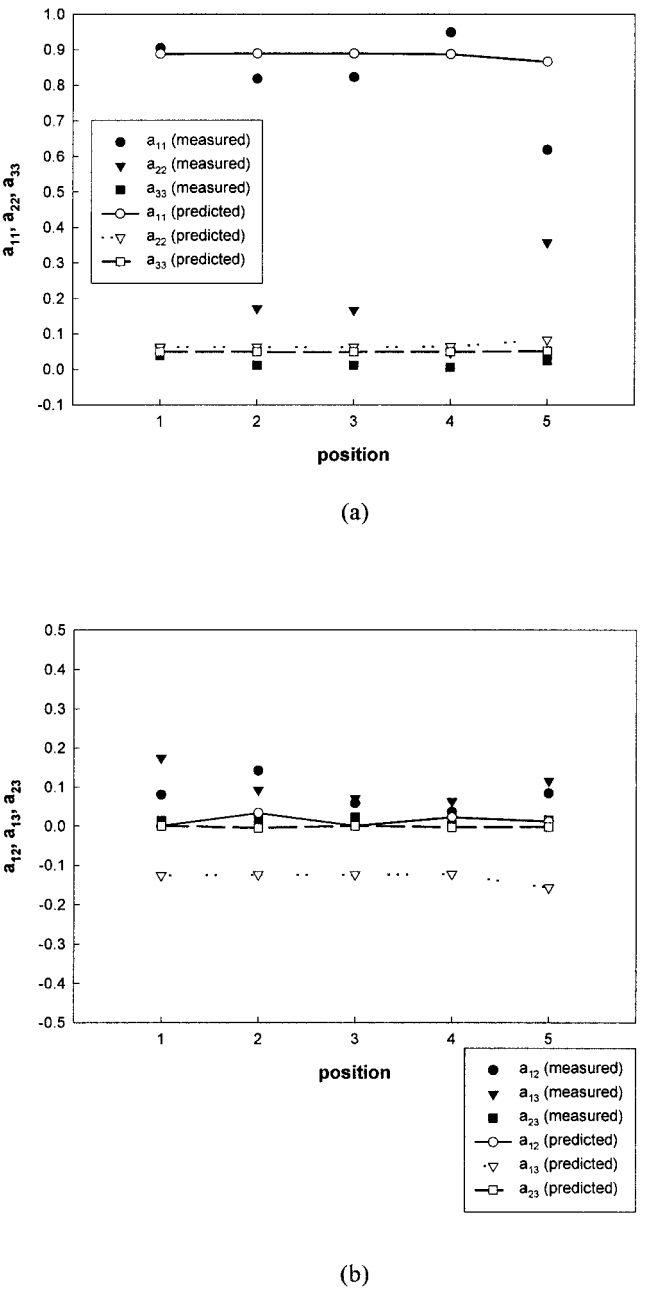

Figure 12 Measured and predicted orientation tensors along location **f:** (a) diagonal components, (b) off-diagonal components.

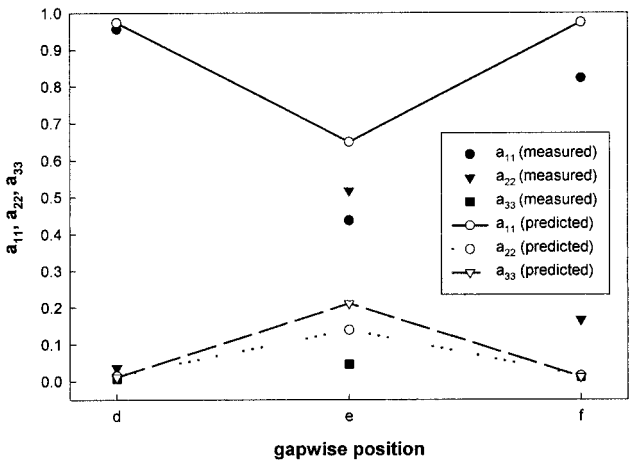

(a)

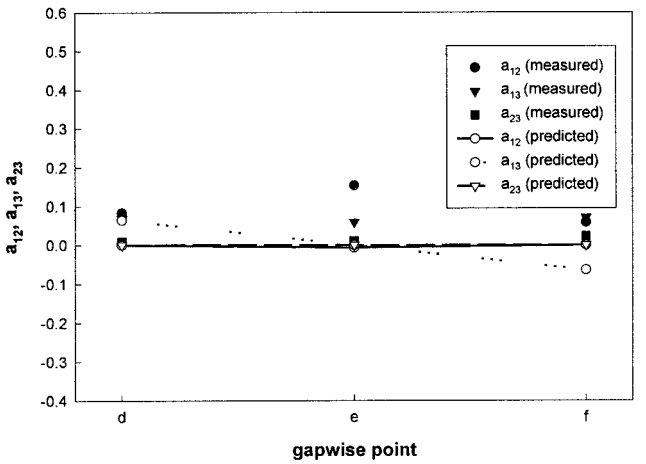

(b)

Figure 13 Measured and predicted orientation tensor with respect to the thickness at the center of position 3: (a) diagonal components, (b) off-diagonal components.

y-direction. Fibers are highly aligned to the flow direction at positions 3 and 4 and are rather randomly oriented at the end of specimen. Although the degree of fiber alignment in the flow direction varies slightly in the measured data, the predicted orientation shows the same tendency as the measured one through positions 1 to 4. There is substantial discrepancy at the end of specimen. In Figure 12, a_{11} component measured at position 3 is smaller than that predicted by the numerical analysis. It is believed that the discrepancy results from the effect of fountain flow, which has not been taken into account in the numerical simulation.

Orientation states with respect to thickness

A shell–core structure[23,24] appears at the center of position 3 as shown in Figure 13. Since orientation of fibers near the wall is affected by strong shear flow, most fibers are aligned along the flow direction. On the other hand, fibers near the core are randomly oriented because shear deformation rates are reduced and some elongational effects in the thickness direction are present. There is a rather significant discrepancy in a_{11} component at the center location e between measured and predicted values. The predicted valued is higher that the measured one because the fountain flow effect is not considered in the numerical prediction.

Visual representation of orientation states

Since nonzero off-diagonal components indicate that reference x-, y-, and z-axes are not the principal axes,[25] it is very complicated to interpret the orientation states

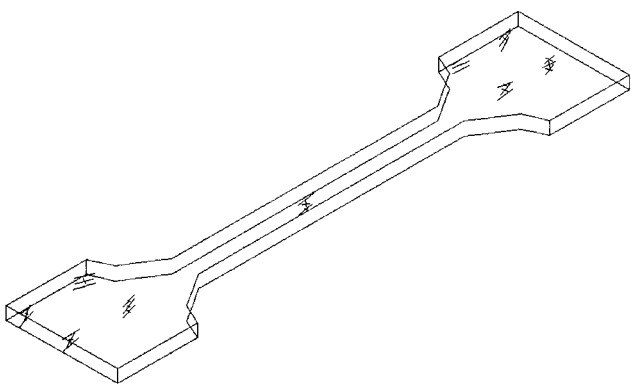

(a)

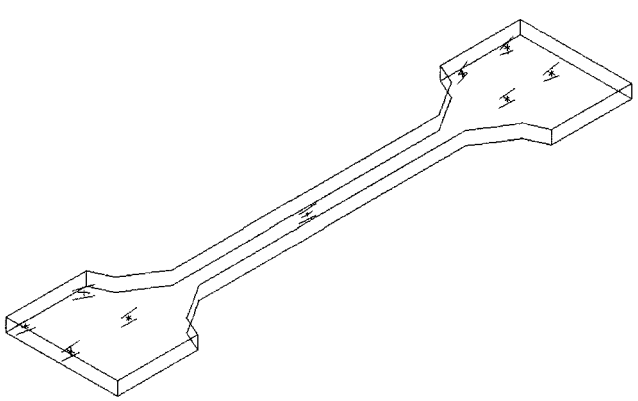

(b)

Figure 14 Three-dimensional representation of the principal directions of measured orientation tensors.

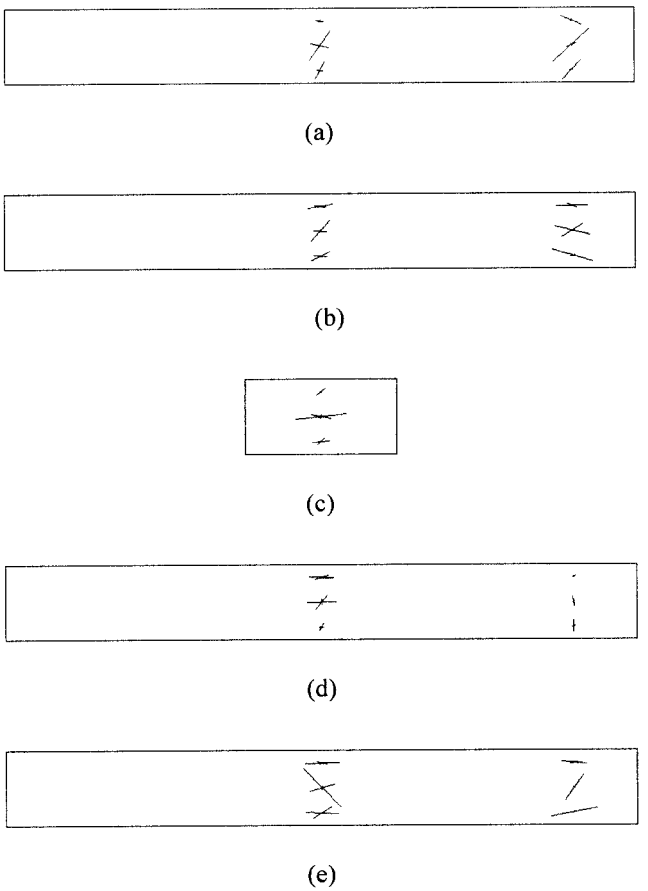

Figure 15 Principal directions of measured orientation tensors projected onto the y–z plane: (a) position 1, (b) position 2, (c) position 3, (d) position 4, (e) position 5.

from the tensors when nonzero values in off-diagonal occur. However, using eigenvectors and eigenvalues of the orientation tensors makes it easy to interpret the orientation states because eigenvectors of the orientation tensor can represent three-dimensional orientation states.[26] The eigenvectors of the tensor denote principal directions of orientation and corresponding eigenvalues indicate degree of orientation in their eigenvector directions. Therefore, projections of the eigenvectors on any surface can be used to describe the orientation state in that plane.

Figures 14 and 15 show the visual representation of three-dimensional orientation state by using eigenvectors and eigenvalues. Each line represents eigenvector of the orientation tensor and the length of each line equals magnitude of the corresponding eigenvalue. Here, the length of each line is taken to be twice the eigenvalue for good visualization. Overall orientation states of the specimen are shown in Figure 14 and those projected onto the y–z plane are shown in Figure 15.

CONCLUSIONS

Employment of CLSM makes it possible to remove the ambiguity in determining the off-diagonal components of orientation tensors and to measure fully three-dimensional fiber orientation states in SFRP. The orientation tensors are obtained at different positions of the tensile specimen along the flow direction as well as on the cross section normal to the flow direction. In general, the specimen has the shell–core structure, where fibers are highly aligned to the flow direction near the mold wall and randomly oriented in the middle of the specimen. From near the gate to the converging region, fibers are rotated from one direction to the other along the corner of the specimen. At the end of the cavity, random orientation state is developed in the core. The predicted orientation tensors generally show good agreement with the measured ones along the corner and top and bottom surfaces of the part. Although tensile specimens are characterized in this study, it is crucial to obtain three-dimensional orientation states of complicated parts in order to bring off the relationship between processing conditions, internal structures, and physical properties of the part.

References

1. Ko, J.; Youn, J. R. Polym Comp 1995, 16, 114.
2. Lee, S. C.; Yang, Y.; Ko, J.; Youn, J. R. J Mat Proc Tech 1997, 70, 83.
3. Chung, D. H.; Kwon, T. H. Korea-Australia Rheo J 2000, 12, 125.
4. Lee, S. W.; Youn, J. R. Macromolec Symp 1999, 148, 211.
5. Lee, K. H.; Youn, J. R. Polym Comp 1992, 13, 251.
6. Shim, H. H.; Kwon, O. K.; Youn, J. R. Wear 1992, 157, 141.
7. Shim, H. H.; Kwon, O. K.; Youn, J. R. Polym Comp 1990 11, 337.
8. Yurgartis, S. W. Comp Sci Tech 1987, 30, 279.
9. Hine, P. J.; Davidson, N.; Duckett, R. A.; Clarke, A. R.; Ward, I. M. Polym Comp 1996, 17, 720.
10. Avérous, L.; Quantin, J. C.; Crespy, A.; Lafon, D. Polym Eng Sci 1997, 37, 329.
11. McGrath, J. J.; Wille, J. M. Comp Sci Tech 1995, 53, 133.
12. Thomason, J. L.; Knoester, A. J Mater Sci Lett 1990, 9, 258.
13. McGee, S. H.; McCullough, R. L. J Appl Phys 1984, 55, 1394.
14. Advani, S. G.; Tucker, C. L., III. J Rheol 1987, 31, 751.
15. Bay, R. S.; Tucker, C. L., III. Polym Eng Sci 1992, 32, 240.
16. Clarke, A. R.; Archenhold, G.; Davidson, N. C. Comp Sci Tech 1995, 55, 75.
17. Clarke, A. R.; Archenhold, G.; Davidson, N. C. In Microstructural Characterisation of Fibre-Reinforced Composites; Summerscales, J. Ed.; Woodhead: Cambridge, UK, 1998; Chapter 7.
18. Lee, S. W. MS Thesis, Seoul National University, 1997.
19. Advani, S. G.; Tucker, C. L., III. J Rheol 1990, 34, 367.
20. Lee, Y. H. MS Thesis, Seoul National University, 1999.
21. Jain, A. K. Fundamentals of Digital Image Processing; Prentice Hall: Englewood Cliffs, NJ, 1989.
22. Yang, H.; Colton, J. S. Polym Comp 1994, 15, 46.
23. Bay, R. S.; Tucker, C. L., III. Polym Comp 1992, 13, 317.
24. Bay, R. S.; Tucker, C. L., III. Polym Comp 1992, 13, 332.
25. Tucker, C. L., III; Advani, S. G. In Flow and Rheology in Polymer Composites Manufacturing; Advani, S. G. Ed.; Elsevier: Amsterdam, 1994; Chapter 6.
26. Altan, M. C.; Subbiah, S.; Güçeri, S. I.; Pipes, R. B. Polym Eng Sci 1990, 30, 848.